Antitumor and Antivascular Effects of AVE8062 in Ovarian Carcinoma

Tae Jin Kim,[1,5] Murali Ravoori,[2] Charles N. Landen,[1] Aparna A. Kamat,[1] Liz Y. Han,[1] Chunhua Lu,[1] Yvonne G. Lin,[1] William M. Merritt,[1] Nicholas Jennings,[1] Whitney A. Spannuth,[1] Robert Langley,[2] David M. Gershenson,[1] Robert L. Coleman,[1] Vikas Kundra,[3,4] and Anil K. Sood[1,2]

Departments of [1]Gynecologic Oncology, [2]Cancer Biology, [3]Experimental Diagnostic Imaging, and [4]Radiology, University of Texas M. D. Anderson Cancer Center, Houston, Texas; and [5]Division of Gynecologic Oncology, Department of Obstetrics and Gynecology, Cheil General Hospital, and Women's Healthcare Center, Kwandong University College of Medicine, Seoul, Korea

Abstract

The purpose of this study was to examine the therapeutic efficacy and underlying mechanisms of action of a vascular-disrupting agent, AVE8062, and to determine its effects on tumor metabolic activity. The *in vitro* and *in vivo* effects of AVE8062 alone and in combination with docetaxel were tested in chemotherapy-sensitive and chemotherapy-resistant ovarian cancer models. Tumors were analyzed for necrosis, microvessel density, endothelial cell apoptosis, and proliferation following treatment. The effect of AVE8062 on tumor regression and metabolic activity was examined by magnetic resonance (MR) or by [^{18}F]fluorodeoxyglucose ([^{18}F]FDG) uptake by positron emission tomography (PET) with MR imaging, respectively. AVE8062 monotherapy was effective in inhibiting tumor growth in all models (range 43–51% versus control; $P < 0.05$). Combination therapy was even more effective in inhibiting tumor growth (range 76–90% compared with controls, $P < 0.01$). AVE8062 in combination with chemotherapy significantly prolonged survival in HeyA8-injected mice ($P < 0.001$) compared with other groups. AVE8062-based therapy resulted in rapid development of central tumor necrosis, decreased microvessel density, decreased proliferation, and induction of apoptosis of tumor-associated endothelial cells. MR imaging showed regression of established HeyA8 ovarian tumors and [^{18}F]FDG PET with MR showed rapid decrease in metabolic activity after AVE8062 therapy. Combination of AVE8062 plus docetaxel results in potent inhibition of ovarian cancer growth. These results suggest that AVE8062 may be useful as a clinical therapeutic approach for ovarian cancer patients and that functional [^{18}F]FDG PET imaging may predict clinical response before an anatomic reduction in tumor size. [Cancer Res 2007;67(19):9337–45]

Introduction

Ovarian cancer remains the most common cause of death from a gynecologic malignancy. In 2007, it is estimated that over 22,430 women will develop ovarian cancer and 15,280 will die as a result (1). The high mortality associated with ovarian cancer is thought to be due to the advanced stage of disease at presentation. Despite improvements in surgical and chemotherapeutic approaches, most patients develop recurrent disease, where long-term survival rates remain dismal. Thus, novel therapeutic strategies are needed to improve the outcome of this deadly disease.

It is well established that tumor cells depend on the presence of a functional blood vessel network for their growth, survival, and metastatic spread (2, 3). Tumor vasculature is a promising target for novel anticancer agents because endothelial cells are thought to be genetically stable compared with tumor cells. In addition, tumor vasculature seems to be functionally different from normal vasculature. For example, tumor vessels exhibit a more tortuous course, greater leakiness, and disorganized blood flow (4). Thus, targeting the phenotypic differences between tumor and normal vasculature is attractive because it has the potential to be effective against bulky established tumors, which are often considered to be resistant to conventional chemotherapy. Vascular-disrupting agents (VDA) are a relatively new class of drugs that cause a rapid and extensive shutdown of established tumor vasculature, leading to secondary tumor cell death characterized by early and extensive tumor cell necrosis (5).

Combretastatin A-4 (CA-4; refs. 6–8), its disodium phosphate salt (CA-4 prodrug; refs. 9, 10), ZD6126 (prodrug of *N*-acetylcolchinol; ref. 11), and AVE8062 (a derivative of CA-4 prodrug; ref. 12) are tubulin-binding agents that belong to a new family of small molecular weight drugs possessing potent antivascular properties (6–10). They are structurally related to the colchicines, which are a class of naturally occurring toxic alkaloids whose biological function seems to occur through microtubule polymerization. Although the specific mechanisms underlying the antivascular effects of this new class of agents are not fully understood, similar properties have been seen with other tubulin-binding microtubule-disrupting agents such as the *Vinca* alkaloids (5) and the taxanes (13). The effects of these agents include morphologic alterations in endothelial cells mediated by disruption and reorganization of microtubules, and a rapid increase in tumor vascular permeability mediated by disruption and reorganization of the actin cytoskeleton (6–10). However, it is not fully known whether such vascular-targeting agents also have direct effects on tumor cells. Thus, in the current study, we considered both the antivascular and antitumor effects of AVE8062. The therapeutic efficacy of AVE8062 was examined alone and in combination with standard chemotherapy in multiple orthotopic models of ovarian cancer. Furthermore, to assess whether early functional imaging could predict therapeutic response to AVE8062, we used [^{18}F]FDG positron emission tomography (PET) imaging.

Note: Supplementary data for this article are available at Cancer Research Online (http://cancerres.aacrjournals.org/).

V. Kundra and A.K. Sood contributed equally to this work.

Requests for reprints: Anil K. Sood, Departments of Gynecologic Oncology and Cancer Biology, University of Texas M. D. Anderson Cancer Center, 1155 Herman Pressler, Unit 1362, Houston, TX 77030. Phone: 713-745-5266; Fax: 713-792-7586; E-mail: asood@mdanderson.org.

doi:10.1158/0008-5472.CAN-06-4018

Materials and Methods

Cell lines and culture. The ovarian cancer cell lines HeyA8 and SKOV3ip1 (14) were maintained in RPMI 1640 supplemented with 15% fetal bovine serum (FBS) and 50 μg/mL gentamicin sulfate (Gemini Bioproducts). The HeyA8-MDR cell line, a taxane-resistant line (a kind gift from Dr. Isaiah J. Fidler, Department of Cancer Biology, University of Texas M. D. Anderson Cancer Center, Houston, TX), was maintained in the above medium with 300 μg/mL of paclitaxel. Endothelial cells isolated from the mesentery of the immortomouse [mouse mesenteric endothelial cell (MMEC)] were maintained in DMEM supplemented with 10% FBS and 0.01% gentamicin sulfate. These cells proliferate indefinitely by means of SV40 transformation at 33°C, but not at 37°C (15). Before the experiments, these cells were kept at 37°C for 48 h to allow elimination of SV40 expression. All cell lines were routinely screened for *Mycoplasma* species (GenProbe detection kit; Fisher). All experiments were done with 70% to 80% confluent cultures.

Orthotopic *in vivo* model and tissue processing. Female athymic nude mice (6–8 weeks old) were purchased from the National Cancer Institute-Frederick Cancer Research and Development Center and housed in specific pathogen-free conditions. They were cared for in accordance with guidelines set forth by the American Association for Accreditation of Laboratory Animal Care and the USPHS Policy on Human Care and Use of Laboratory Animals; and all studies were approved and supervised by the M. D. Anderson Cancer Center Institutional Animal Care and Use Committee. For *in vivo* injection, tumor cells were trypsinized, centrifuged at 1,000 rpm × 7 min at 4°C, washed twice, and resuspended in serum-free HBSS (Life Technologies) at a concentration of 5×10^6 cells/mL (SKOV3ip1 and HeyA8-MDR) and 1.25×10^6 cells/mL (HeyA8). Tumors were established by i.p. injection of cells. AVE8062 (Sanofi-Aventis) therapy was initiated 7 or 17 days after cell line injection. Mice (n = 10 per group) were randomly assigned to the following treatment groups: (*a*) PBS 200 μL, i.p. weekly; (*b*) AVE8062 30 mg/kg [dissolved in PBS (pH 5)] i.p. twice weekly; (*c*) docetaxel 2 mg/kg (HeyA8 and HeyA8-MDR) or 1.4 mg/kg (SKOV3ip1) i.p. weekly; (*d*) AVE8062 plus docetaxel (both drugs given at the doses and frequency described above for each drug alone). The dose of AVE8062 used in these experiments was optimized from dose-escalation studies against tumor growth. Mice were monitored for signs of adverse effects and tumors were harvested after treatment (range 2–5 weeks). The mouse weight, tumor weight, number of tumor nodules, and volume of ascites were recorded at necropsy.

Immunohistochemistry. Formalin-fixed, paraffin-embedded sections were deparaffinized in xylene, rehydrated in graded alcohol, and transferred to PBS. After citrate buffer (pH 6.0) antigen retrieval, endogenous peroxidase was blocked with 3% hydrogen peroxide in methanol for 12 min. Nonspecific epitopes were blocked with fragment block (1:10, Jackson ImmunoResearch Laboratories) overnight at 4°C. After additional blocking with 5% normal horse serum (NHS) and 1% normal goat serum (NGS) at room temperature, sections were incubated with the monoclonal mouse anti–PCNA (proliferating cell nuclear antigen)-PC10 antibody (1:50; DAKO) at room temperature for 3 h followed by incubation with horseradish peroxidase (HRP)–conjugated rat anti-mouse IgG2a (1:100, Serotec, Harlan Bioproducts for Science, Inc.) for 1 h at room temperature. PCNA was determined by the percentage of PCNA-positive cells in 10 high-powered fields at ×100.

Terminal deoxyribonucleotide transferase (TdT)–mediated nick-end labeling (TUNEL) staining was done after deparaffinization and treatment with proteinase K (1:500). One slide with DNase (1:50) was used as a positive control. All slides were then treated with 3% H_2O_2/methanol for 12 min, rinsed with distilled water, and then incubated with TdT buffer for 2 min. Next, samples were incubated with terminal transferase (1:400) and biotin-16-dUTP (1:200) in TdT buffer at 37°C for 1 h. After blocking with 2% bovine serum albumin, visualization was achieved with peroxidase streptavidin (1:400, DAKO) at 37°C for 40 min. TUNEL was quantified by the number of TUNEL-positive cells in 10 randomly selected samples at ×100.

CD31 immunohistochemistry was done on freshly cut frozen sections. After fixation with cold acetone, acetone + chloroform (1:1), and acetone, samples were incubated with 1:800 of rat monoclonal anti-mouse CD31 (1:800, PharMingen) overnight at 4°C followed by HRP-conjugated goat anti-rat IgG (1:200, Jackson ImmunoResearch Laboratories). Visualization was achieved with 3,3′-diaminobenzidine (Research Genetics) and counterstaining with Gil's hematoxylin (BioGenex Laboratories). Microvessel density was quantified by the number of lumen-like structures adjacent to CD31-positive endothelial cells. All images were captured using a three-chip camera (Sony Corporation) and the Optimas Image Analysis software (Bioscan).

Confocal immunofluorescence for CD31 (endothelial cells) and TUNEL (apoptotic cells). Eight-micrometer-thick frozen tissues were fixed in cold acetone, acetone/chloroform (1:1), and acetone, followed by blocking with 5% NHS and 1% NGS in PBS for 20 min at room temperature. Sections were then incubated with rat anti-CD31 antibody (1:400, PharMingen) for 18 h at 4°C and then with Texas red AffiniPure goat IgG (1:200, Jackson ImmunoResearch Laboratories). After washing with PBS and PBS + 0.1% Brij, TUNEL staining was done on the same samples using a commercially available apoptosis detection kit (DeadEnd Fluorometric TUNEL System, Promega Corporation). Samples were fixed with 4% paraformaldehyde for 10 min at room temperature, washed with PBS, then incubated with 0.2% Triton X-100 for 15 min and with equilibration buffer for 10 min. Next, sections were incubated for 1 h in a 37°C darkened humidity chamber with nucleotide mix and TdT enzyme in equilibration buffer. The reaction was terminated by immersing the samples in 2× SSC for 15 min. Unincorporated fluorescein dUTP was removed, and samples were then incubated with 100 ng/mL of Hoechst stain for 10 min to quantify endothelial cells. Immunofluorescence microscopy was done using a ×20 objective (Zeiss Plan-Neofluar) on an epifluorescence microscope (Ludl Electronic Products). Images were captured using a cooled charge-coupled device camera (Photometrics) and Smart Capture software (Digital Scientific). Endothelial cells were identified by red fluorescence, and DNA fragmentation was detected by localized green and yellow fluorescence within the nucleus of apoptotic endothelial cells. Quantification of apoptotic endothelial cells was expressed as an average of the ratio of apoptotic endothelial cells to the total number of endothelial cells in 10 randomly selected 0.039-mm^2 fields at ×200.

***In vitro* cytotoxicity assay**. Two thousand tumor cells were seeded into 38-mm^2 wells of flat-bottomed 96-well plates in triplicate and allowed to adhere overnight. Cultures were then washed and regular medium (negative control) or medium containing docetaxel with or without AVE8062 were added. After 72 h, the number of metabolically active cells was determined by 3-(4,5-dimethylthiazol-2-yl)-2,5-diphenyltetrazolium bromide (MTT) assay. Dose-response curves for growth inhibition were generated as a percentage of untreated control. IC_{50} was determined by nonlinear least-squares regression (Prism, Graph Pad Software, Inc.). Combination assays were done by using the IC_{50} of AVE8062 (7–20 nmol/L, depending on the cell line) with escalating doses of docetaxel. To assess the potential effect of combination AVE8062 and docetaxel therapy relative to either agent alone, dose-response curves were compared. The null hypothesis was that the IC_{50} values were shared. To confirm a differential benefit for the combination, the curves were reanalyzed constraining the IC_{50} to the best performing single agent.

Analysis of cell cycle and apoptosis by flow cytometry. The capacity of AVE8062 to modulate MMEC and HeyA8 cell cycle as well as apoptosis was analyzed by flow cytometry. In all assays, 3×10^6 tumor cells were seeded into Petri dishes and allowed to adhere overnight. The cultures were then washed with PBS and treated with regular medium (negative control) or medium containing docetaxel, AVE8062 (HeyA8, 20 nmol/L; MMEC 10 nmol/L), or AVE8062 plus docetaxel. For cell cycle analyses, tumor cells were collected by trypsinization and pooled with the cells floating in the medium. The cell suspensions were centrifuged for 5 min at 1,500 rpm at room temperature, then washed and fixed with ethanol. For apoptosis analysis, cells were incubated overnight in 50 μL of DNA labeling solution (10 μL of reaction buffer, 0.75 μL of TdT enzyme, 8 μL of FITC-dUTP, and 32.25 μL of distilled water) at room temperature. Following the addition of rinse buffer, samples were centrifuged, washed, and fixed in ethanol. All samples were then washed with PBS, then resuspended in propidium iodide (50 μg/mL) and RNase A (20 μg/mL) in PBS for 30 min at room

temperature. Stained cells were analyzed on an EPICS XL flow cytometer (Beckman-Coulter). The low-level gate was set at the base of the G_1 peak and the percentages of cells within the G_1 and G_2-M phases of the cell cycle were determined by analysis with Multicycle (Phoenix Flow Systems).

Magnetic resonance imaging of i.p. tumor. Initial magnetic resonance (MR) imaging of i.p. tumors was done 14 to 15 days after injection of 2.5×10^5 HeyA8 tumor cells. On day 17, treatment with AVE8062 (30 mg/kg, i.p., twice weekly) was initiated. To assess the effect on tumor growth after AVE8062 treatment, repeat MR imaging was done on days 24 to 25. All mice were sacrificed 1 to 2 days after MR imaging to record tumor weight. Weight derived from MR images was correlated with weight measured *ex vivo*. For all MR imaging experiments, animals were anesthetized with 2% isoflurane. Imaging was done in a 4.7-T small-animal MR scanner (Biospec, Bruker Biospin Corp.). A T_2-weighted fast spin echo sequence (echo time, 70 ms; repetition time, 2,088 ms; nex 3; field of view, 3.7 × 5 cm; matrix, 256 × 256; spatial resolution, 195 μm) was used to acquire images in sagittal and coronal planes. Using the Image J program (NIH), tumor measurements were done using coronal images. Regions of interest (ROI) were drawn on each image containing tumor and then multiplied by slice thickness to obtain the tumor volume. If the tumor was seen in several slices, then tumor volumes were added together. To control for volume averaging, one half of the volume of tumor from the most dorsal and ventral images containing the tumor was used in the volume analysis. Assuming a tumor density of 1 g/mL, tumor volumes (mm^3) were converted to weight in grams for analysis (16). The serial imaging allowed longitudinal evaluation of each tumor. The weight of each tumor on day 25 was subtracted from the weight of the same tumor on day 15 to obtain the difference in tumor weight.

MR and PET imaging of i.p. tumor. After AVE8062 treatment, MR and PET imaging were done 19 to 20 days after i.p. injection of 2.5×10^5 HeyA8 cells. On day 21, [^{18}F]FDG PET imaging was done. The next day, mice were treated with a single dose of AVE8062 (30 mg/kg i.p.) or PBS (n = 5–8 mice per group) and PET imaging was done serially 2 and 24 h after treatment. Mice were sacrificed after final PET imaging and tumor weights were recorded.

For all PET imaging, anesthetized mice were injected i.v. with 150 μCi of [^{18}F]FDG. Thirty minutes later, animals anesthetized with 2% isofluorane were imaged for 15 min using a microPET Rodent R4 scanner (Concorde Microsystems, Inc.). Images were reconstructed using OSEM2D (Ordered Subsets Expectation Maximization) software provided by the manufacturer. ROI (counts per pixel per minute) were converted to microcuries using a calibration curve derived from scanning standard activity phantoms in the microPET scanner. [^{18}F]FDG uptake by each tumor was divided by the weight of the tumor derived from MR imaging to obtain %ID/g for each mouse.

Statistical analysis. Comparisons of tumor weight and quantification of PCNA, TUNEL, CD31, percentage of necrotic portion, and percentage of apoptotic endothelial cells were analyzed by two-tailed Student's t test or ANOVA (for all groups) if normally distributed, and the Mann-Whitney rank sum test or Kruskal-Wallis test (for all groups) if nonparametric. Differences between groups were considered statistically significant if $P < 0.05$. For *in vivo* therapy experiments, 10 mice in each group were used based on a power analysis to detect a 50% reduction in tumor size (β error 0.2). Survival curves were plotted using the Kaplan-Meier method and compared with the log-rank test. Linear regression was used to analyze correlations of tumor weight derived by MR versus that of excised tumors.

Results

***In vivo* efficacy of AVE8062.** Before performing therapy experiments, we tested the tolerability of various doses of AVE8062 ranging from 10 to 100 mg/kg given twice weekly via i.v., i.p., or s.c. routes in nude mice (n = 3 per group). The i.v. and s.c. routes were not pursued further due to problems with skin or tail vein necrosis. The i.p. route was well tolerated with doses up to 100 mg/kg. Next, preliminary experiments were done to determine the lowest dose for *in vivo* therapeutic efficacy. Starting 7 days after tumor cell injection, nude mice (n = 5 per group) bearing HeyA8 ovarian cancer cells were treated with either vehicle or AVE8062 10, 30, 50, and 100 mg/kg twice weekly i.p. for 3 weeks. There was 65% reduction in tumor weight in the 30 mg/kg group compared with the vehicle control group ($P < 0.02$; data not shown). The 10 mg/kg dose was not effective. The antitumor effects at doses >30 mg/kg were not significantly better; therefore, the 30 mg/kg dose was selected for subsequent therapy experiments.

Effect of AVE8062 and docetaxel on ovarian tumor growth *in vivo*. To determine the therapeutic potential of AVE8062, extensive analyses were done using orthotopic models of advanced ovarian cancer. To simulate advanced disease, therapy was initiated 1 week (early treatment) after tumor cell injection, with animals divided into four groups (10 mice per group): (*a*) vehicle alone; (*b*) AVE8062 30 mg/kg twice weekly; (*c*) docetaxel 2 mg/kg (HeyA8 and HeyA8-MDR) or 1.4 mg/kg (SKOV3ip1) weekly; and (*d*) AVE8062 plus docetaxel (both drugs given at the doses and frequency described above for each drug alone). The mice were treated for 3 to 5 weeks (depending on the cell line tested) and sacrificed when the mice in the control group were moribund. In the HeyA8 model, AVE8062 treatment alone resulted in 43% reduction in tumor size compared with control ($P = 0.04$) and docetaxel alone resulted in 68% reduction ($P = 0.03$; Fig. 1*A*). In comparison, the combination therapy had the greatest efficacy, resulting in 86% inhibition ($P = 0.008$). Similar results were noted with the SKOV3ip1 model, with 45% reduction in tumor growth with AVE8062 alone ($P = 0.01$) and 90% reduction in combination with docetaxel ($P < 0.001$; Fig. 1*A*).

Despite high response rates to primary chemotherapy, most ovarian cancer patients eventually develop recurrent disease, which becomes refractory to chemotherapy (17). Therefore, we also examined the effects of AVE8062 on the taxane-resistant HeyA8-MDR cell line. In this model, AVE8062 treatment alone reduced tumor growth by 51% ($P = 0.008$) compared with the controls (Fig. 1*A*). As expected, docetaxel treatment alone did not alter tumor growth. However, the combination of AVE8062 with docetaxel was superior to all other groups in inhibiting tumor growth (76%; $P < 0.001$).

Given that many patients with recurrent ovarian cancer have bulky disease, we next evaluated the effects of AVE8062 in mice with a larger HeyA8 tumor burden. For these experiments, treatment was started 17 days after tumor cell injection (palpably ~0.75 cm tumors). AVE8062 treatment resulted in a 35% reduction in tumor burden ($P = 0.04$), but docetaxel alone had no effect. However, even in this model of bulkier disease, the combination treatment resulted in 80% smaller tumor size versus vehicle control ($P = 0.001$; Fig. 1*A*).

Based on the encouraging results with regard to *in vivo* tumor growth inhibition, we next examined the effects of single-agent AVE8062, docetaxel, and combination AVE8062/docetaxel on survival. In this experiment, therapy was initiated 1 week after HeyA8 inoculation and continued until each animal became moribund. AVE8062 alone did not improve survival compared with control (Fig. 1*B*). However, docetaxel alone and in combination with AVE8062 yielded a significant survival advantage over control or AVE8062 alone ($P < 0.001$). Treatment with both drugs (AVE8062 and docetaxel) was well tolerated, and there were no significant differences in mouse body weight between the groups tested (data not shown).

Assessment of tumor size (MR imaging) and metabolism ([^{18}F]FDG PET). We used longitudinal MR imaging to determine

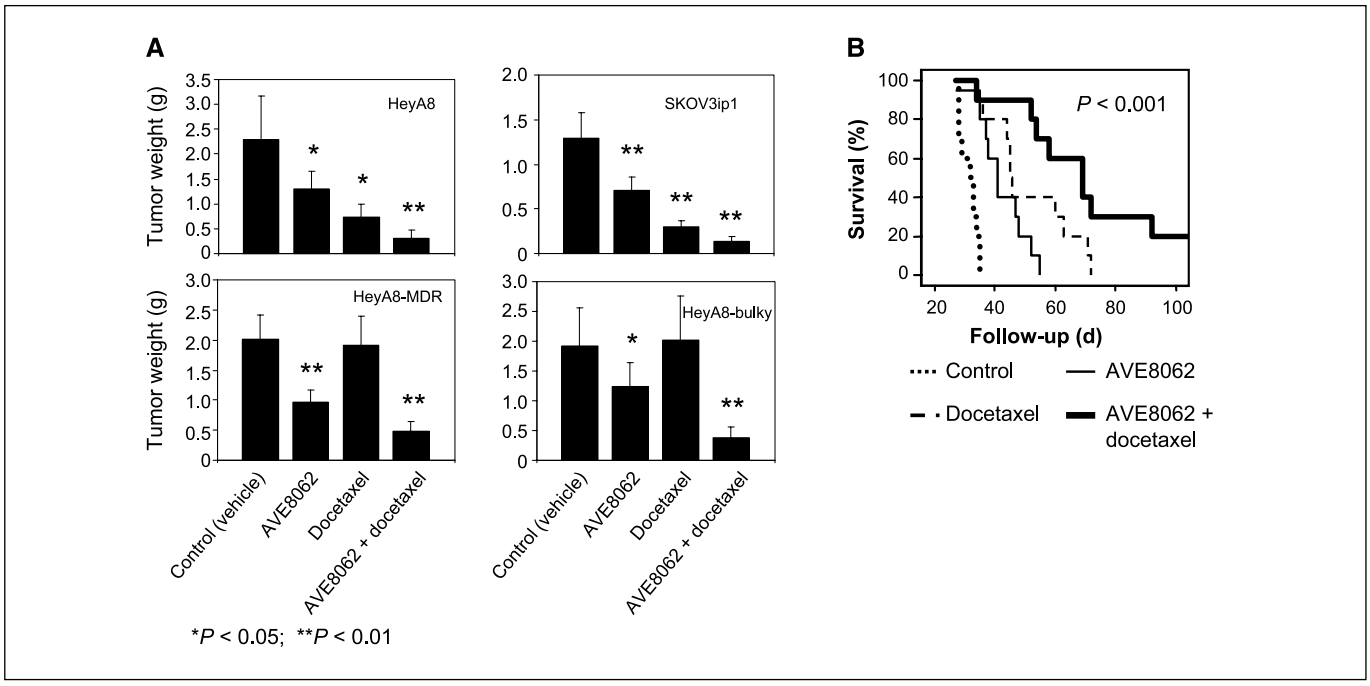

Figure 1. Therapeutic efficacy of AVE8062 with docetaxel. *A,* nude mice inoculated i.p. with either HeyA8, SKOV3ip1, or HeyA8-MDR were randomly allocated to one of the following groups (n = 10 per group), with therapy beginning 1 wk after tumor cell injection: vehicle control, AVE8062, docetaxel, and AVE8062 + docetaxel. For experiments with HeyA8-formed tumors (*HeyA8-bulky*), treatment was started 17 d after tumor cell inoculation. The animals were sacrificed when control mice became moribund (3–5 wks after start of treatment). *B,* Kaplan-Meier survival of HeyA8-inoculated mice based on the four therapy groups noted above (n = 10 per group). The equality of survival curves was tested using the log-rank statistic.

the effects of AVE8062 on formed tumors (Fig. 2*A*). We first measured tumor size and weight using MR imaging 14 to 15 days after i.p. injection of HeyA8 tumor cells and 10 days after initiation of AVE8062 30 mg/kg i.p. twice weekly. Tumor weight derived from MR imaging on days 24 to 25 correlated highly with that from excised tumors (r = 0.97, P < 0.001, n = 12; Fig. 2*B*). Treated mice showed significant reductions in tumor size compared with control (P < 0.01, n = 6 per group; Fig. 2*C*), suggesting that AVE8062 is indeed effective in the treatment of bulkier tumors.

Based on the known ability of AVE8062 to induce vascular collapse, we next asked whether this would also result in a rapid decrease in the metabolic activity of tumors, as assessed by [^{18}F]FDG PET. To assess tumor weight, nude mice bearing HeyA8 tumors (n = 6) were imaged on days 19 to 20 by MR. For functional imaging, a baseline [^{18}F]FDG PET examination was done 21 days after tumor implantation. The next day, AVE8062 30 mg/kg was given i.p. and imaging was repeated at 2 and 24 h after treatment. The [^{18}F]FDG uptake by PET and tumor weight derived by MR were used to determine %ID/g for each tumor at the pretreatment, 2 and 24 h time points after AVE8062 therapy. At 2 and 24 h, %ID/g decreased by 83% (P < 0.01) and 82% (P < 0.01), respectively, compared with pretreatment for the AVE8062-treated animals (Fig. 2*D*); however, no difference was noted in the vehicle-treated control group.

Antivascular effects of AVE8062. To evaluate potential mechanisms to explain the efficacy of AVE8062, we examined the extent of tumor necrosis, microvessel density (CD31), proliferation (PCNA), and apoptosis (TUNEL) in tumors from either the therapy experiments described above or short-term experiments done separately. To quantitate the extent of necrosis, the entire excised tumor was fixed, stained with H&E, and scanned. The necrotic portion was quantified by pixel counts after a single dose of AVE8062 alone or in combination with docetaxel in mice bearing formed HeyA8 ovarian tumors (17 days after i.p. injection of tumor cells). AVE8062 monotherapy resulted in ~30% necrosis compared with 7.7% in the controls (P = 0.01; Fig. 3*A*). The combination of docetaxel and AVE8062 resulted in the greatest necrosis (74% necrosis; P < 0.001). We also examined the extent of necrosis in the SKOV3ip1 model (has numerous, but smaller, modules compared with the HeyA8 model) and observed significant necrosis in both of the AVE8062 treatment groups (Supplementary Fig. S1). Based on the known effects of AVE8062 on endothelial cells, we next determined microvessel density in tumors harvested after 3 weeks of therapy. There was a 54% decrease in microvessel density with AVE8062 monotherapy (P = 0.02), and a 68% decrease when combination therapy was used (P < 0.001; Fig. 3*B*). To determine whether the effects of AVE8062 on endothelial cells were direct, we assessed for endothelial cell apoptosis using dual colocalization of CD31 and TUNEL. Initially, we found no apoptotic endothelial cells in tumors harvested after prolonged therapy (data not shown). It is likely that detecting apoptotic tumor-associated endothelial cells may be difficult after multiple doses of therapy because the majority of AVE8062-sensitive cells would have been affected during earlier treatments (18). Therefore, we examined the effects of AVE8062 therapy on tumors harvested 48 h after a single dose. There was a substantial increase in endothelial cell apoptosis after AVE8062 treatment (Fig. 3*C*; P < 0.001) compared with vehicle control or docetaxel alone. The effect of combination therapy was even more pronounced (P < 0.001) at this earlier time point. The effects of therapy on tumor cell apoptosis were also examined in all four groups. As expected, the greatest effect on tumor cell apoptosis was noted in the combination group (Fig. 3*D*; P < 0.001)

compared with controls. We also evaluated major organs, including kidney, spleen, liver, heart, and lung, for endothelial cell apoptosis after AVE8062 treatment. There was no significant increase in endothelial apoptosis (<1%) in these organs (Supplementary Fig. S2).

Direct effects of AVE8062 on tumor cells. Although the effects of AVE8062 on endothelial cells are known, we next asked whether this agent also has direct effects on ovarian cancer cells. To answer this question, we examined the effects of AVE8062 on endothelial or tumor cell viability using the MTT assay. The IC_{50} of AVE8062 for the MMECs was 10 nmol/L and ranged between 7 and 20 nmol/L for the tumor cell lines (HeyA8, SKOV3ip1, and HeyA8-MDR), as shown in Fig. 4*A*. Comparative analysis of the nonlinear least-squares regression of the dose-response curves for each agent alone and combination AVE8062/docetaxel showed a significantly lower IC_{50} than either agent alone ($P < 0.005$, all cell lines). The cytotoxicity of docetaxel was 2- to 4-fold greater in combination with AVE8062 for the endothelial and tumor cells compared with docetaxel alone (Fig. 4*A*). The effects of AVE8062 on *in vivo* proliferation were assessed in tumors harvested from the therapy experiments described above using PCNA stains. Representative pictures and mean PCNA counts are presented in Fig. 4*B*. The control tumors had 53% proliferating tumor cells compared with 34% in the AVE8062 group ($P = 0.03$) and 24% in the docetaxel group ($P = 0.005$). Tumors treated with combination showed an even greater reduction in proliferation rate (15%), which is significantly reduced compared with either treatment alone ($P < 0.001$). These findings indicate that the *in vivo* effects on proliferation are likely reflective of both antitumor and antiendothelial effects.

AVE8062 causes G_2-M phase arrest. To determine potential mechanisms of AVE8062-induced cell death, we examined cell cycle and apoptosis using flow cytometry in endothelial and tumor cells. In mesenteric endothelial cells, treatment with AVE8062 resulted in G_2-M arrest of 60% within 8 h compared with 13% for controls ($P < 0.001$; Fig. 5*A*). In HeyA8 cells, the increase in G_2-M arrest was observed at a later time (60% at 24 h, $P < 0.01$ compared with vehicle control; Fig. 5*B*). As expected, AVE8062 alone and in combination with docetaxel resulted in a significant increase in MMEC apoptosis compared with the vehicle control or docetaxel-alone groups ($P < 0.01$; Fig. 5*C*). In the HeyA8 cell line, increase in apoptosis was observed at a later time (48 h; $P < 0.01$; Fig. 5*D*).

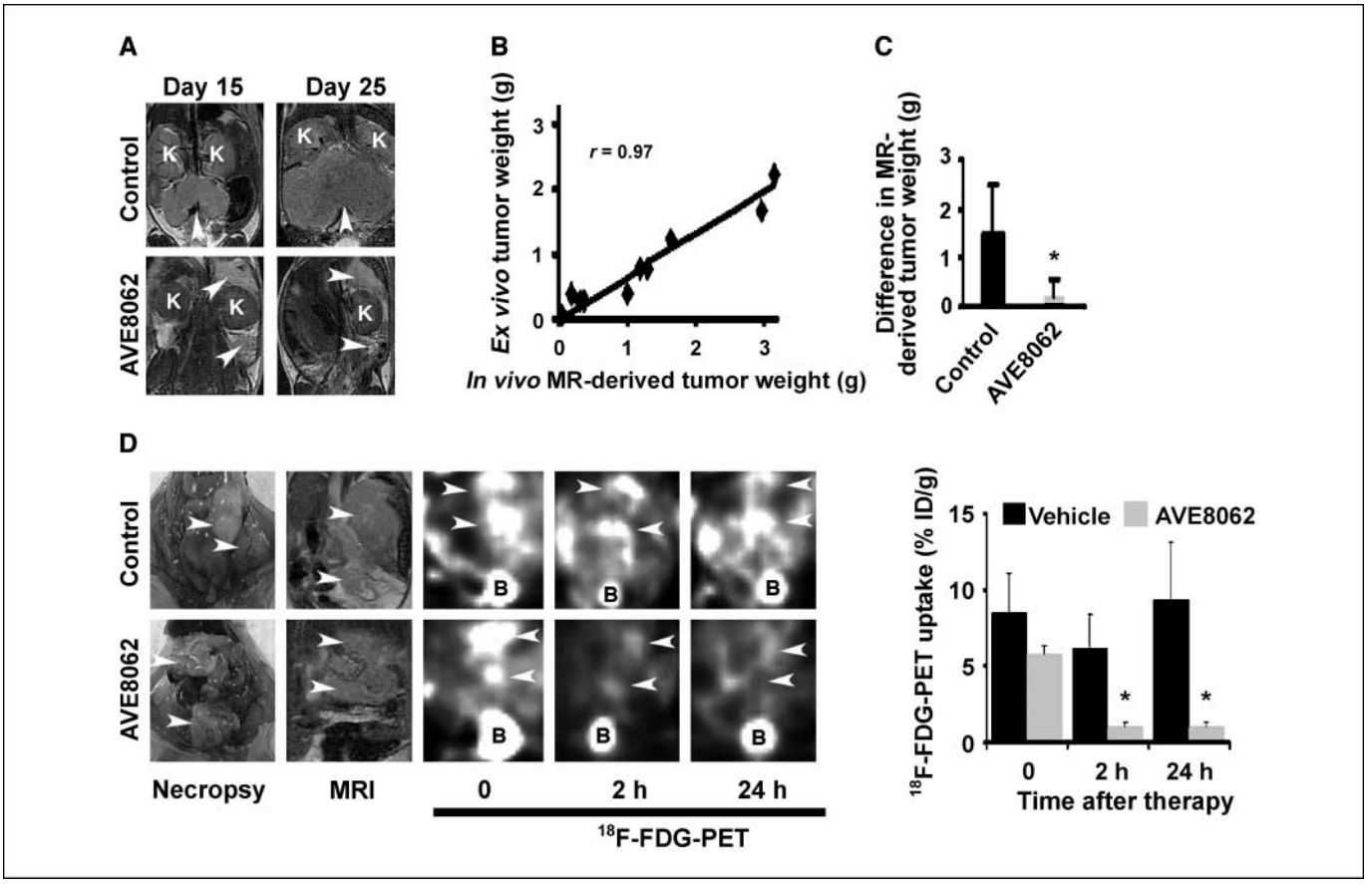

Figure 2. *A, in vivo* MR imaging shows that AVE8062 reduces the growth of established HeyA8 tumors. Representative coronal MR images of mice before or after treatment with vehicle or AVE8062. MR imaging was done on days 15 and 25 after HeyA8 inoculation. Treatment with AVE8062 at a dose of 30 mg/kg i.p. twice weekly or vehicle was begun on day 17. MR used a T_2-weighted fast spin echo sequence. *Arrowhead,* tumor; *K,* kidney. *B,* regression analysis shows that tumor weight derived from MR imaging correlates with the weight of excised tumors ($r = 0.97$). *C,* difference in tumor weight derived from serial MR images of the animals described in *A* (*$P < 0.01$). *D,* AVE8062 reduces [^{18}F]FDG uptake within 24 h of therapy. Representative, coronal necropsy, MR, and [^{18}F]FDG PET images of nude mice (representative control and treatment group mice are shown). MR imaging using a T_2-weighted fast spin echo sequence was done 3 wks after HeyA8 inoculation. Subsequently, [^{18}F]FDG PET imaging was done before, 2 h, and 24 h after a single dose of AVE8062 at 30 mg/kg i.p. or vehicle. *Arrowhead,* tumor. *B,* bladder. [^{18}F]FDG uptake (%ID/g) before, 2 h, and 24 h after treatment with AVE8062 is shown graphically on the right. *Bars,* SD. *, $P < 0.01$ when comparing %ID/g posttreatment with pretreatment.

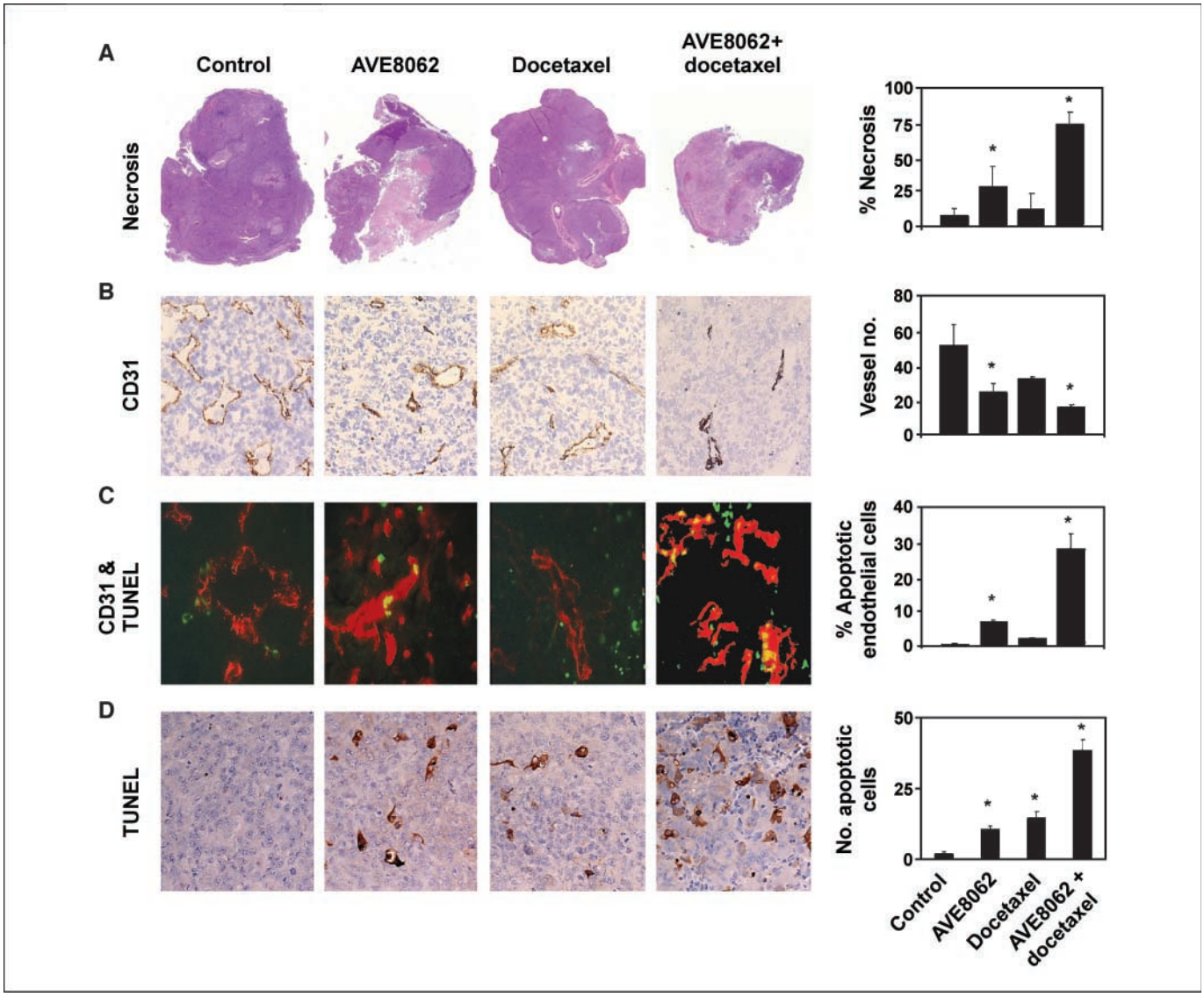

Figure 3. *A,* assessment of tumor necrosis. The entire tumor from each therapy group was fixed, stained with H&E, and scanned. The necrotic portion was quantitated by pixel counts using Adobe Photoshop. *B,* microvessel density was determined after immunohistochemical peroxidase staining for CD31 and the number of vessels per ×100 field was determined (after 3–5 wks of therapy). Representative slides from each group are shown, and the average numbers of vessels per field are shown in the graph. Ten fields per slide and at least three slides per group were examined. *C,* assessment of endothelial cell apoptosis in ovarian carcinoma (48 h after start of therapy). Representative images of immunofluorescence staining with CD31-positive cells (*red*) and cells undergoing apoptosis (TUNEL stain; *green*). *D,* representative images of TUNEL immunohistochemistry from each group. The number of apoptotic cells was counted. *Columns,* mean of TUNEL-positive cells; *bars,* SE. Ten fields per slide and at least three slides per group (from different animals) were counted. The columns in all of the graphs correspond to the labeled columns in the picture. *, $P \leq 0.01$.

Discussion

In the present study, we have shown that the vascular-targeting agent AVE8062 in combination with a conventional cytotoxic agent, docetaxel, is highly efficacious in ovarian carcinoma. The efficacy was documented in both developing and established tumors in multiple orthotopic ovarian cancer mouse models. These effects are due to direct effects on both tumor and associated endothelial cells. Furthermore, [^{18}F]FDG PET imaging predicted tumor response as early as 2 h after AVE8062 therapy. These results are clinically relevant as a significant unmet need in the management of ovarian cancer is novel agent discovery, which has the potential to overcome intrinsic and acquired drug resistance to conventional cytotoxic chemotherapy, particularly in established and often bulky tumor nodules. In addition, if validated in humans, early measures of efficacy for this class of agents can protect patients from receiving multiple courses of ineffective therapy.

The efficacy of VDAs such as CA-4 phosphate and ZD6126 has been reported in some preclinical models, including colon and lung cancer (19–21). Previous reports evaluating the combination of VDAs and conventional chemotherapy have shown enhanced tumor response without an apparent increase in host toxicity (22–35). For instance, Goto et al. (25) reported that ZD6126 combined with cisplatin significantly reduced tumor weight and number of metastatic nodules in a human lung cancer orthotopic model without concomitant organ toxicity. Similarly, Seimann and Rojiani (23, 24) documented antitumor efficacy of ZD6126 combined with cisplatin in a s.c. rodent sarcoma and human renal cancer model. The current report is the first to evaluate the

antitumoral effects of AVE8062 alone and in combination with docetaxel in an orthotopic model of ovarian cancer.

AVE8062 is a derivative of CA-4 phosphate, which is known to exhibit antivascular effects through selective disruption of the tubulin cytoskeleton of endothelial cells (11, 36–38). The molecular mechanisms underlying these effects are not well characterized; however, microtubule targeting activates the mitotic spindle checkpoint that monitors chromosome attachment to the mitotic spindle and delays chromosome segregation during anaphase until defects in the mitotic spindle apparatus are corrected. Because mitotic arrest (G_2M) induced by VDAs frequently precedes apoptosis, it is widely hypothesized that this arrest is the primary stimulus for apoptosis (36–38). In addition to this direct cytotoxic effect, an antivascular mechanism seems to be mediated via endothelial cell cytoskeletal reorganization and cell shape changes resulting in vascular collapse, increased permeability, and decreased tumor perfusion. Direct effects on tumor cells have been suggested *in vivo*, but to the best of our knowledge, have not been directly shown previously (39). Our finding of direct antitumoral effects is important as targeted therapy to both tumor and host provides a robust platform upon which to develop novel therapeutics and strategies.

To assess the potential utility of AVE8062 alone and in combination with docetaxel, we initially did efficacy experiments *in vivo* with small volume orthotopic models of ovarian cancer.

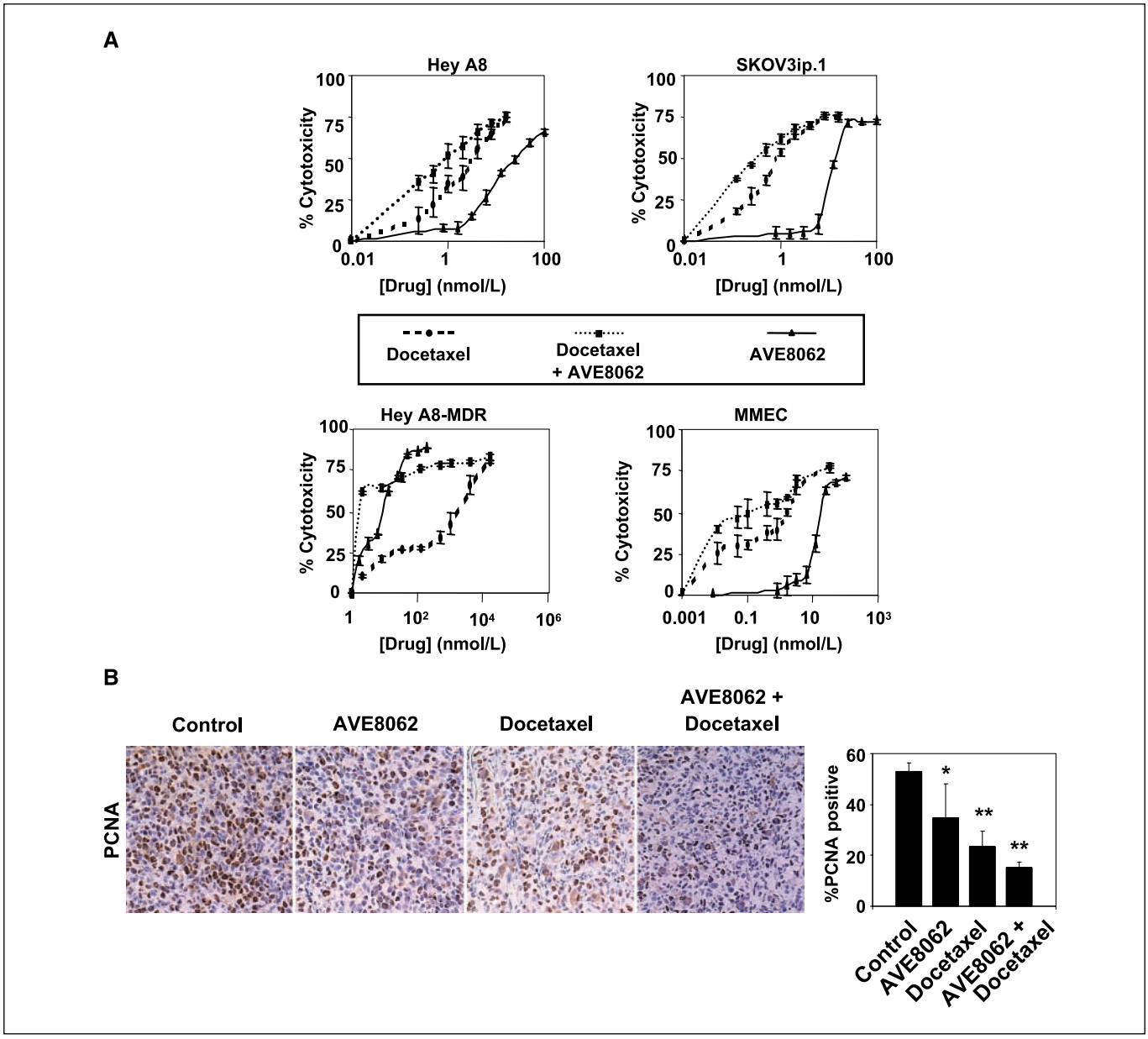

Figure 4. *A,* effect of AVE8062 alone or in combination with docetaxel on ovarian cancer cell cytotoxicity: HeyA8, SKOV3ip1, HeyA8-MDR, or MMEC cells were plated in 96-well plates and treated for 72 h. Cell viability was determined with the MTT assay. *Points,* means of three independent experiments; *bars,* SE. *B,* tumor sections from each of the four *in vivo* therapy groups were stained for PCNA. The number of cancer cell nuclei that were strongly PCNA positive were counted and divided by the total number of cells. Representative images from each group (original magnification, ×100). *Columns,* mean percentage of PCNA-positive cells; *bars,* SE. Ten fields per slide and at least three slides per group (from different animals) were counted. The columns in all of the graphs correspond to the labeled columns in the picture. *, $P < 0.05$; **, $P \leq 0.01$.

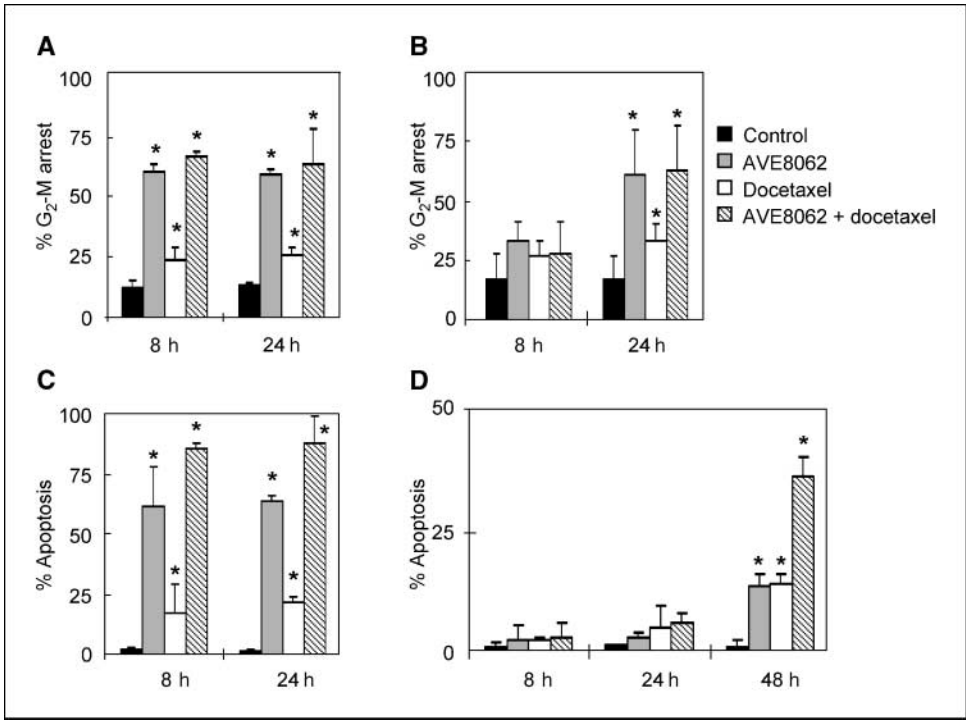

Figure 5. Distribution of MMEC (*A*) and HeyA8 (*B*) cells in G_2-M phase of cell cycle was established by flow cytometry. *Columns,* mean of three determinations; *bars,* SE. Effects of AVE8062 and docetaxel on *in vitro* apoptosis of MMEC (*C*) and HeyA8 cells (*D*). The percentage of apoptosis was determined by TUNEL assay. Cells were treated with IC_{50} concentration of both drugs. *Columns,* means of three independent experiments; *bars,* SE. *, $P \leq 0.01$.

Significant reductions in tumor weight were observed for each of the treatment cohorts with the expected exception of single-agent docetaxel in the HeyA8-MDR model. The importance of evaluating the combination of AVE8062 and docetaxel in a drug-resistant model is to parallel the frequently observed clinical challenge of acquired resistance. In addition to established efficacy *in vivo*, we observed remarkably enhanced antitumor effects with docetaxel in this model, suggesting that the two agents would be a relevant therapeutic choice in a mixed sensitivity population of tumor present in bulky disease or generated by exposure to prior cytotoxic therapy. This effect was indeed observed in our *in vivo* therapy experiment in the bulky HeyA8 orthotopic tumor model. In these experiments, docetaxel monotherapy was not effective and was similar to the HeyA8-MDR model.

Describing the mechanisms for these encouraging therapeutic outcomes is necessary to understand how the target tissues are affected and to aid in strategic drug development. We approached this facet from several angles to not only evaluate the effects of therapy anatomically (excised tumors), but also metabolically ([^{18}F]FDG PET imaging). Our longitudinal imaging protocols mimicked the serial imaging that is done in the clinic to monitor individual tumors in patients before and after therapy. Tozer et al. (40) have previously shown rapid vascular shutdown after treatment with CA-4P in a mouse model of carcinosarcoma. The resultant increase in hematocrit, increased viscosity, and increased interstitial pressure led to vascular occlusion followed by tumor cell kill. In the current report, we extend these findings by substantial and early effects on metabolic activity, as assessed by [^{18}F]FDG PET imaging. Therefore, it is possible that [^{18}F]FDG PET may be an early indicator of therapeutic response with AVE8062 and other vascular-targeting agents.

In addition to antivascular effects on endothelial cells, we hypothesized that AVE8062 might have direct cytotoxic effects on tumor cells. To evaluate this, we studied induced cell cycle effects *in vitro* on ovarian cancer cells. AVE8062 arrested tumor cells in G_2-M and induced apoptosis. The correlation between time of detectable mitotic arrest and apoptosis suggests that the latter occurs after a relatively short period of mitotic shutdown. This effect augmented the *in vitro* efficacy of docetaxel as documented by the 2- to 4-fold reduction in IC_{50} for docetaxel in the presence of AVE8062 in our cytotoxicity experiments. Enhanced efficacy with the AVE8062 and docetaxel combination was observed in each of our models, including the taxane-resistant HeyA8-MDR cell line. The pronounced effect is felt to be primarily due to apoptosis after mitotic arrest (41, 42).

Development of VDAs, as a new class of therapeutic agents, is ongoing via early clinical investigation. Our observations support the strategy of combining these agents with a cytotoxic agent. Because at least additive effects are observed with taxanes, these regimens are highly desirable in ovarian cancer management. However, an early phase trial of CA-4-P and carboplatin documented higher than expected hematologic toxicity, predominantly thrombocytopenia, highlighting the necessity to design trials with careful pharmacokinetic studies to evaluate the potential for drug-drug interactions (43). In the current study, we identified a potential dose threshold for AVE8062 from which additional dose escalation did not improve cytotoxicity. Because MTD-based studies are usually defined by attendant toxicity in dose escalation, consideration of optimal biological doses through early *in vivo* imaging will be desirable. In addition, given the observed effects on endothelium and tumor cells, investigation on wound healing will be necessary to establish safety. Future experiments to optimize therapeutic efficacy may include varying dosing schedules such as temporally separating administration of a second drug relative to administration of AVE8062. Nonetheless, our documentation of augmented cytotoxicity even in a drug-resistant model is an encouraging factor for future clinical development.

In summary, we have documented that AVE8062 inhibits ovarian cancer growth through direct effects on endothelial cells causing substantive disruption in tumor blood flow leading to central necrosis in our orthotopic murine model. The effects are rapid in onset and clearly seen by noninvasive PET imaging. We documented the effects on developing tumors and, perhaps more importantly, in established tumors and among both taxane-sensitive and taxane-resistant tumors. These data indicate that AVE8062 in combination with chemotherapy may offer opportunities for novel therapeutic strategies in ovarian carcinoma.

Acknowledgments

Received 10/31/2006; revised 6/19/2007; accepted 7/23/2007.

Grant support: National Cancer Institute/Department of Health and Human Services/NIH Training of Academic Gynecologic Grant T32-CA101642 (Y.G. Lin, W.M. Merritt, and W.A. Spannuth); the University of Texas M. D. Anderson Cancer Center Specialized Programs of Research Excellence in ovarian cancer grant P50CA83639; NIH grants CA109298 and CA110793; the Marcus Foundation Grant (A.K. Sood); and the Cancer Center Support (CORE) Grant P30CA-016672, Small Animal Imaging Facility from the NIH.

The costs of publication of this article were defrayed in part by the payment of page charges. This article must therefore be hereby marked *advertisement* in accordance with 18 U.S.C. Section 1734 solely to indicate this fact.

References

1. American Cancer Society. Cancer facts and figures—2007. Atlanta (GA): American Cancer Society; 2007.
2. Folkman J, Shing Y. Angiogenesis. J Biol Chem 1992; 267:10931–4.
3. Folkman J. Seminars in Medicine of the Beth Israel Hospital, Boston. Clinical applications of research on angiogenesis [comment]. N Engl J Med 1995;333:1757–63.
4. Fukumura D, Yuan F, Monsky WL, Chen Y, Jain RK. Effect of host microenvironment on the microcirculation of human colon adenocarcinoma. Am J Pathol 1997; 1151:679–88.
5. Tozer GM, Kanthou C, Baguley BC. Disrupting tumour blood vessels. Nat Rev Cancer 2005;5:423–35.
6. Pettit GR, Singh SB, Hamel E, Lin CM, Alberts DS, Garcia-Kendall D. Isolation and structure of the strong cell growth and tubulin inhibitor combretastatin A-4. Experientia 1989;45:209–11. Erratum in: Experientia 1989;45:680.
7. Tozer GM, Kanthou C, Parkins CS, Hill SA. The biology of the combretastatins as tumour vascular targeting agents. Int J Exp Pathol 2002;83:21–38.
8. Dark GG, Hill SA, Prise VE, Tozer GM, Pettit GR, Chaplin DJ. Combretastatin A-4, an agent that displays potent and selective toxicity toward tumor vasculature. Cancer Res 1997;57:1829–34.
9. Tozer GM, Prise VE, Wilson J, et al. Combretastatin A-4 phosphate as a tumor vascular-targeting agent: early effects in tumors and normal tissues. Cancer Res 1999; 59:1626–34.
10. Galbraith SM, Maxwell RJ, Lodge MA, et al. Combretastatin A4 phosphate has tumor antivascular activity in rat and man as demonstrated by dynamic magnetic resonance imaging. J Clin Oncol 2003;21: 2831–42.
11. Davis PD, Dougherty GJ, Blakey DC, et al. ZD6126: a novel vascular-targeting agent that causes selective destruction of tumor vasculature. Cancer Res 2002;62: 7247–53.
12. Nihei Y, Suga Y, Morinaga Y, et al. A novel combretastatin A-4 derivative, AC-7700, shows marked antitumor activity against advanced solid tumors and orthotopically transplanted tumors. Jpn J Cancer Res 1999;90:1016–25.
13. Browder T, Butterfield CE, Kraling BM, et al. Antiangiogenic scheduling of chemotherapy improves efficacy against experimental drug-resistant cancer. Cancer Res 2000;60:1878–86.
14. Yu D, Wolf JK, Scanlon M, Price JE, Hung MC. Enhanced c-erbB-2/neu expression in human ovarian cancer cells correlates with more severe malignancy that can be suppressed by E1A. Cancer Res 1993;53:891–8.
15. Langley RR, Ramirez KM, Tsan RZ, Van Arsdall M, Nilsson MB, Fidler IJ. Tissue-specific microvascular endothelial cell lines from H-2K(b)-tsA58 mice for studies of angiogenesis and metastasis. Cancer Res 2003;63:2971–6.
16. Yang D, Han L, Kundra V. Exogenous gene expression in tumors: noninvasive quantification with functional and anatomic imaging in a mouse model. Radiology 2005;235:950–8.
17. Cannistra SA. Cancer of the ovary. N Engl J Med 2004; 351:2519–29.
18. McCarty MF, Wey J, Stoeltzing O, et al. ZD6474, a vascular endothelial growth factor receptor tyrosine kinase inhibitor with additional activity against epidermal growth factor receptor tyrosine kinase, inhibits orthotopic growth and angiogenesis of gastric cancer. Mol Cancer Ther 2004;3:1041–8.
19. Iyer S, Chaplin DJ, Rosenthal DS, Boulares AH, Li LY, Smulson ME. Induction of apoptosis in proliferating human endothelial cells by the tumor-specific anti-angiogenesis agent combretastatin A-4. Cancer Res 1998;58:4510–4.
20. Boehle AS, Sipos B, Kliche U, Kalthoff H, Dohrmann P. Combretastatin A-4 prodrug inhibits growth of human non-small cell lung cancer in a murine xenotransplant model. Ann Thorac Surg 2001;71: 1657–65.
21. Holwell SE, Cooper PA, Thompson MJ, et al. Anti-tumor and anti-vascular effects of the novel tubulin-binding agent combretastatin A-1 phosphate. Anticancer Res 2002;22:3933–40.
22. Chaplin DJ, Pettit GR, Hill SA. Anti-vascular approaches to solid tumor therapy: evaluation of combretastatin A4 phosphate. Anticancer Res 1999;19: 189–95.
23. Siemann DW, Horsman MR. Enhancement of radiation therapy by vascular targeting agents. Curr Opin Investig Drugs 2002;3:1660–5.
24. Siemann DW, Warrington KH, Horsman MR. Targeting tumor blood vessels: an adjuvant strategy for radiation therapy. Radiother Oncol 2000;57:5–12.
25. Goto H, Yano S, Matsumori Y, Ogawa H, Blakey DC, Sone S. Sensitization of tumor-associated endothelial cell apoptosis by the novel vascular-targeting agent ZD6126 in combination with cisplatin. Clin Cancer Res 2004;10:7671–6.
26. Lash CJ, Li AE, Rutland M, Baguley BC, Zwi LJ, Wilson WR. Enhancement of the anti-tumour effects of the antivascular agent 5,6-dimethylxanthenone-4-acetic acid (DMXAA) by combination with 5-hydroxytryptamine and bioreductive drugs. Br J Cancer 1998;78: 439–45.
27. Cliffe S, Taylor ML, Rutland M, Baguley BC, Hill RP, Wilson WR. Combining bioreductive drugs (SR 4233 or SN 23862) with the vasoactive agents flavone acetic acid or 5,6-dimethylxanthenone acetic acid. Int J Radiat Oncol Biol Phys 1994;29:373–7.
28. Pruijn FB, van Daalen M, Holford NH, Wilson WR. Mechanisms of enhancement of the antitumour activity of melphalan by the tumour-blood-flow inhibitor 5,6-dimethylxanthenone-4-acetic acid. Cancer Chemother Pharmacol 1997;39:541–6.
29. Grosios K, Loadman PM, Swaine DJ, Pettit GR, Bibby MC. Combination chemotherapy with combretastatin A-4 phosphate and 5-fluorouracil in an experimental murine colon adenocarcinoma. Anticancer Res 2000;20: 229–33.
30. Nelkin BD, Ball DW. Combretastatin A-4 and doxorubicin combination treatment is effective in a preclinical model of human medullary thyroid carcinoma. Oncol Rep 2001;8:157–60.
31. Li L, Rojiani AM, Siemann DW. Preclinical evaluations of therapies combining the vascular targeting agent combretastatin A-4 disodium phosphate and conventional anticancer therapies in the treatment of Kaposi's sarcoma. Acta Oncol 2002;41:91–7.
32. Bissery MC, Vrignaud P. *In vivo* synergy between platinum and AVE8062A, a tumor vasculature targeting agent. 94th Annual Meeting of American Association for Cancer Research, Washington DC; 2003.
33. Vrignaud P, Lejeune P, Nicolas S, Bissery MC. *In vivo* synergy between doxorubicin or vinorelbine and AVE8062A, a tumor vasculature targeting agent. 95th Annual Meeting of American Association for Cancer Research, Orlando, FL; 2004.
34. Lejeune P, Vrignaud P, Goulaouic H, Nicolas S, Bissery MC. *In vivo* synergy between docetaxel and AVE8062A, a tumor vasculature targeting agent. 96th Annual Meeting of American Association for Cancer Research, Orange County, CA; 2005.
35. Demers B, Vrignaud P, Bissery MC. *In vivo* synergy combining oxaliplatin with AVE8062A, a vascular-disrupting agent. ASCO Annual Meeting Proceedings 2006:3074.
36. Woods CM, Zhu J, McQueney PA, Bollag D, Lazarides E. Taxol-induced mitotic block triggers rapid onset of a p53-independent apoptotic pathway. Mol Med 1995;1: 506–26.
37. Jordan MA, Wendell K, Gardiner S, Derry WB, Copp H, Wilson L. Mitotic block induced in HeLa cells by low concentrations of paclitaxel (Taxol) results in abnormal mitotic exit and apoptotic cell death. Cancer Res 1996; 56:816–25.
38. Ye K, Zhou J, Landen JW, Bradbury EM, Joshi HC. Sustained activation of p34(cdc2) is required for noscapine-induced apoptosis. J Biol Chem 2001;276: 46697–700.
39. Ohno T, Kawano K, Sasaki A, et al. Antitumor and antivascular effects of AC-7700, a combretastatin A-4 derivative, against rat liver cancer. Int J Clin Oncol 2002; 7:171–6.
40. Tozer GM, Prise VE, Wilson J, et al. Mechanisms associated with tumor vascular shut-down induced by combretastatin A-4 phosphate: intravital microscopy and measurement of vascular permeability. Cancer Res 2001;61:6413–22.
41. Grosios K, Holwell SE, McGown AT, Pettit GR, Bibby MC. *In vivo* and *in vitro* evaluation of combretastatin A-4 and its sodium phosphate prodrug. Br J Cancer 1999; 81:1318–27.
42. Ahmed B, Van Eijk LI, Bouma-Ter Steege JC, et al. Vascular targeting effect of combretastatin A-4 phosphate dominates the inherent angiogenesis inhibitory activity. Int J Cancer 2003;105:20–5.
43. Bilenker J, Flaherty K, Rosen M, et al. Phase I trial of combretastatin A-4 phosphate with carboplatin. Clin Cancer Res 2005;11:1527–33.